Hierarchical FAU- and LTA-Type Zeolites by Post-Synthetic Design: A New Generation of Highly Efficient Base Catalysts

*Danny Verboekend, Tobias C. Keller, Sharon Mitchell, and Javier Pérez-Ramírez**

Hierarchical FAU- and LTA-type catalysts are prepared by post-synthetic modifications and evaluated in the base-catalyzed Knoevenagel condensation of benzaldehyde with malononitrile. A novel route to attain mesoporous Al-rich zeolites (A and X) is demonstrated, while mesoporous Y and USY zeolites are prepared using recently developed methods. Base functionality is introduced by alkali ion exchange (Cs, Na) or by high-temperature nitridation in ammonia. A thorough characterization of the zeolites' structure, composition, porosity, morphology, and basicity demonstrates that the presence of a secondary mesopore network enhances the ion-exchange efficiency and the structural incorporation of nitrogen. The modified USY zeolites display twice the conversion, while the hierarchical A, X, and Y are up to 10 times more active based on the enhanced accessibility. These results demonstrate that the Knoevenagel condensation takes place predominately at the external surface, highlighting secondary porosity as a key criterion in the design of basic zeolite catalysts.

1. Introduction

Zeolites are a class of aluminosilicate catalysts of paramount importance to the chemical and petrochemical industries. Their unique properties, e.g., strong Brønsted acidity, high surface area, high (hydro)thermal stability, and shape selectivity, combined with an extensive tunability, render them the catalyst of choice in many catalyzed reactions.[1,2] Nevertheless, often only a fraction of their potential is exploited, due to diffusion and access limitations. The size of the micropores (0.3–1 nm) is similar to that of many molecules, enforcing an intracrystalline "single file" diffusion. The latter regime is associated with diffusivities orders of magnitude lower compared to outside the pores, implying an underutilization of the zeolite volume.[3]

To alleviate diffusion limitations, wide-pore zeolites and hierarchical zeolites were conceived.[3–6] Whereas the former class aims at enhancing diffusion in the micropores,[7] hierarchical zeolites facilitate access to the active sites in the micropores using a secondary network of meso- or macropores.[8–13] The increased external surface associated with hierarchical zeolites renders the crystal interior more accessible to large molecules,[14] which is particularly advantageous in the catalytic processing of bulky substrates.[15] Hierarchical zeolites can be obtained by reducing the zeolite crystal in one or more dimensions, resulting in nanometer-sized,[8] two-dimensional,[9,10] or lamellar zeolites,[11] or by introducing intracrystalline mesopores and thereby forming mesoporous crystals.[12,13]

Of the plethora of bottom-up and top-down methods available to prepare hierarchical zeolites,[3–13] base leaching, or desilication, is widely applied owing to its experimental simplicity and to the efficiency of the resulting multiporous crystal.[13] Nevertheless, in many cases, desilication by aqueous NaOH should be considered only part of the post-synthetic modification strategy.[13] For example, in the case of Y zeolites,[16] the execution of a dealumination step prior to base leaching facilitates the desired formation of intracrystalline mesopores. Additionally, mild acid washing has proved of crucial importance to remove Al-rich species residual from alkaline treatment. In the case of steamed and acid-leached USY zeolites,[16,17] the inclusion of pore-directing agents (PDAs) in the alkaline solution permits the introduction of extensive mesoporosity while preventing amorphization. The premeditated use of these tools has enabled the preparation of hierarchical zeolites of numerous framework types over a wide compositional range (i.e., from pure silica down to Si/Al ≈ 4).[13,16] Consequently, Al-rich zeolites, e.g., X or A (Si/Al ≈ 1), pose the last compositional challenge to be amended to hierarchical form by post-synthetic strategies.

Hierarchical X[18] and A[19] zeolites have been obtained using bottom-up strategies, involving costly organic templates that after the synthesis need to be thermally removed. However, it should be emphasized that the commercial synthesis of zeolites with Si/Al < 5 does not involve the use of organic templates as structure-directing agents, which significantly reduces manufacturing expenses (ca. 2–5 USD per kg).[20] The resulting economic constraints infer that most preferably affordable routes, e.g., post-synthetic modifications, should be used to derive their mesoporous analogues.

D. Verboekend, T. C. Keller, Dr. S. Mitchell,
Prof. J. Pérez-Ramírez
Institute for Chemical and Bioengineering
Department of Chemistry and Applied Biosciences
ETH Zurich, Wolfgang-Pauli-Strasse 10
CH 8093, Zurich, Switzerland
E-mail: jpr@chem.ethz.ch

DOI: 10.1002/adfm.201202320

To date, the benefits of hierarchical zeolites have predominantly been established for acid-catalyzed reactions.[21] Comparatively, the application of hierarchical zeolites in base catalysis is limited to isolated cases.[22] In fact, in general zeolites have attracted little attention in base-catalyzed processes. The far-from-hegemonic role of zeolite base catalysts stems from the limited basic strength attainable by ion exchange.[23–25] Stronger basicity can be introduced using more elaborated treatments, such as the deposition of intrazeolitic metal clusters[26] or oxides,[27] or the high temperature treatment of acidic zeolites in gaseous NH_3.[28] Another possible reason for the limited application of zeolites in base catalysis is that often bulky molecules are involved, e.g., fine chemicals, which are unable to enter the zeolite micropores. Accordingly, efforts have focused on the base modification of purely mesoporous materials, such as MCM-41.[24] However, the role of mesopores on the catalytic performance of base-modified zeolites remained virtually unexplored.

Herein, we provide insights into the design of superior hierarchical FAU and LTA-type zeolites for base-catalyzed reactions. Recent strategies are employed to prepare mesoporous Y and USY zeolites, and a novel post-synthetic methodology to introduce mesoporosity into low-silica zeolites X and A is presented. The hierarchical zeolites are transformed by alkali (Cs, Na) ion exchange or nitridation in NH_3 at elevated temperatures, followed by a thorough characterization, and catalytic evaluation in the Knoevenagel condensation of benzaldehyde with malononitrile. Enhanced basicity development and catalytic function highlight the value of auxiliary mesoporosity, providing opportunities for the preparation of more efficient zeolite base catalysts.

Table 1. Sample notation and treatment conditions.

Sample code	Reagent	C [M]	$V_{solution}$ [a)] [$cm^3\ g^{-1}$]	T [°C]	t [h]	Repetitions [#]
DA	H_4EDTA	0.11	15	100	72	1
AT1	NaOH	0.2	30	65	0.5	1
AT2	NaOH+TPABr	0.3 + 0.2	30	65	0.5	1
AW1	Na_2H_2EDTA	0.11	60	100	6	1
AW2	Na_2H_2EDTA	0.11	15	100	6	1
NH_4	KCl followed by	3	13	65	2	4
	NH_4Cl	3	50	65	2	4
Na	$NaNO_3$	0.1	100	25	8	3
Cs	$NaNO_3$ followed by	0.1	100	25	8	3
	CsOAc	0.1	100	25	24	1

a)Volume of solution per gram of zeolite.

2. Results and Discussion

The results and discussion are organized in three sections: Section 2.1 covers the post-synthetic transformation of conventional X, A, Y, and USY zeolites into their hierarchical analogues. Section 2.2 tackles the introduction of basicity into the zeolites by ion exchange or nitridation. Finally, Section 2.3 presents the catalytic benefits of basic hierarchical zeolites in the Knoevenagel condensation of benzaldehyde with malononitrile.

2.1. Mesoporosity Introduction

The transformation of the conventional zeolites to the hierarchical form was performed using the post-synthetic liquid-phase modifications summarized in **Table 1**. Below, the porous modifications of each zeolite (X, A, Y, USY) are described.

Zeolite X: The parent NaX zeolite exhibited a diffraction pattern corresponding to a single-phase highly-crystalline faujasite structure (**Figure 1**), large µm-sized crystals (**Figure 2** and **Figure 3**), and a N_2 adsorption isotherm typical of a conventional microporous zeolite (**Figure 4**a). Consistent with the low Si/Al ratio (≈1.2), no dissolution, crystallinity alteration, or mesopore formation was apparent upon alkaline treatment of the parent sample with 0.2 M NaOH (X-AT1) (**Table 2**). In the case of zeolite Y, the high framework stability in alkaline media can be overcome by a mild dealumination treatment with H_4EDTA to reach a Si/Al of ca. 4. This enables mesopore formation by subsequent desilication in NaOH and acid washing in aqueous Na_2H_2EDTA.[16] However, similar dealumination of zeolite X is not readily achieved without invoking major structural loss.[29] To maintain a high cation exchange capacity (CEC), essential for the introduction of alkali metal ions, reduction of the framework Si/Al ratio should be minimized. Nevertheless, since mesoporosity can also be generated through mild alkaline and acid washings,[16] partial amorphization followed by sequential removal of the resulting debris offers an alternative route to obtain a hierarchical zeolite X by post-synthetic modification.

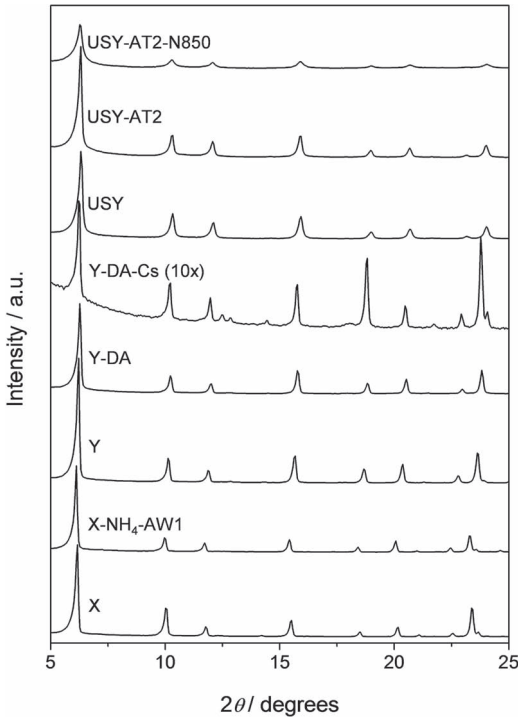

Figure 1. X-ray diffraction patterns of selected faujasite zeolites.

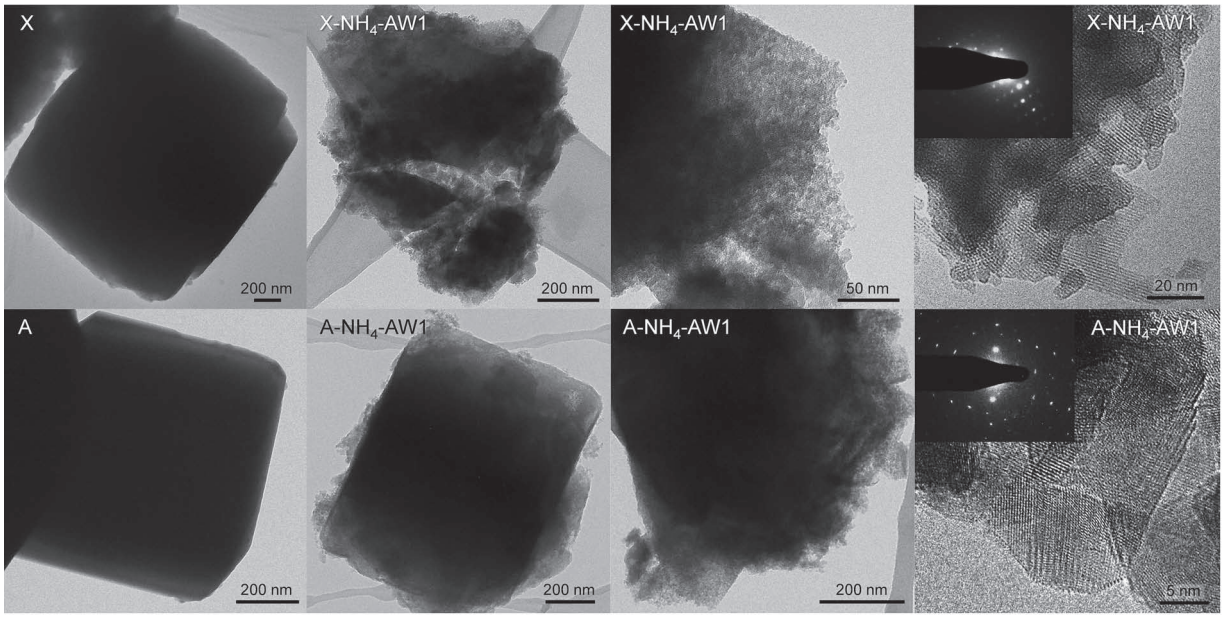

Figure 2. Transmission electron micrographs of conventional and hierarchical X and A zeolites. Insets: selected area diffraction patterns.

To evaluate this hypothesis, zeolite X was first brought to the ammonium form. The resulting zeolite (X-NH_4) displayed a considerably reduced crystallinity (74%), consistent with the relative instability of ammonium-exchanged zeolite X.[30] Subsequent alkaline treatment of this zeolite (X-NH_4-AT1) led to a substantially lower yield than that obtained upon similar treatment of the sodium form (Table 2). However, the mesopore surface area did not exceed 53 m^2 g^{-1}. No improvement

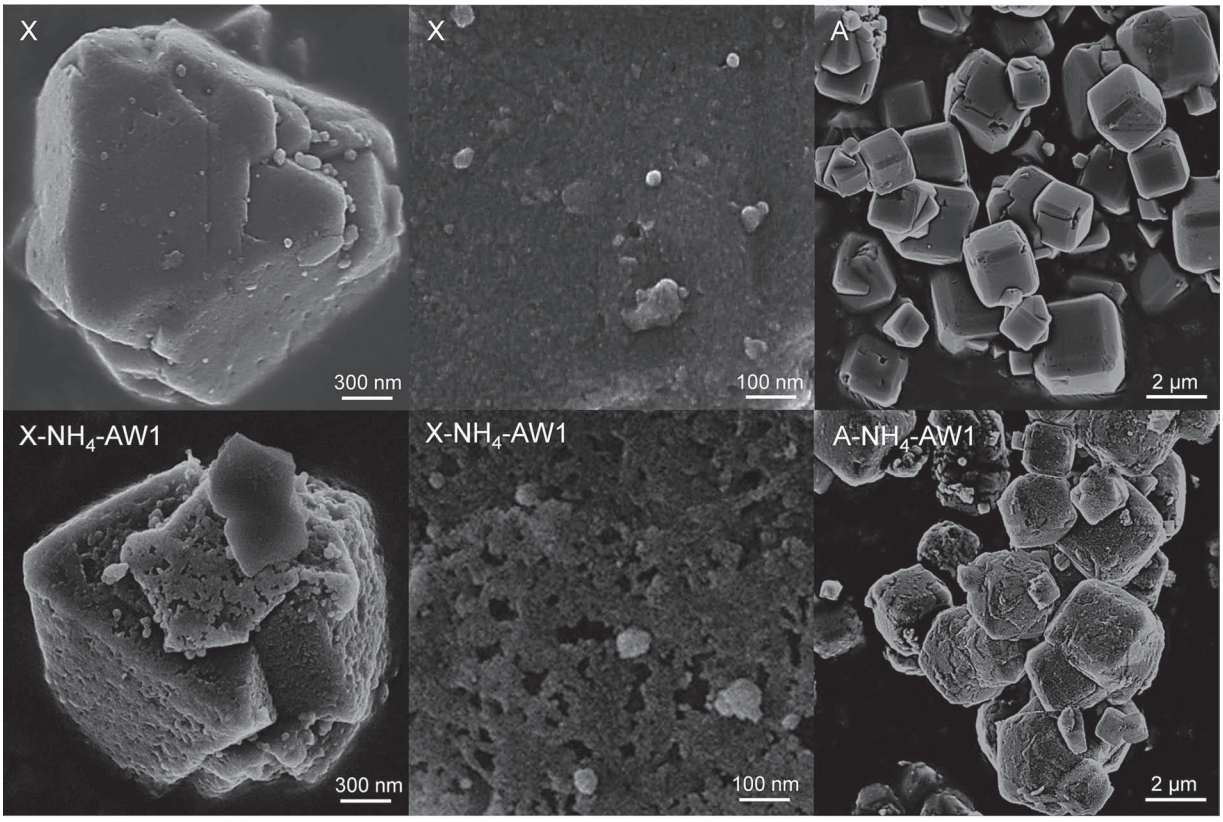

Figure 3. Scanning electron micrographs of conventional and hierarchical X and A zeolites.

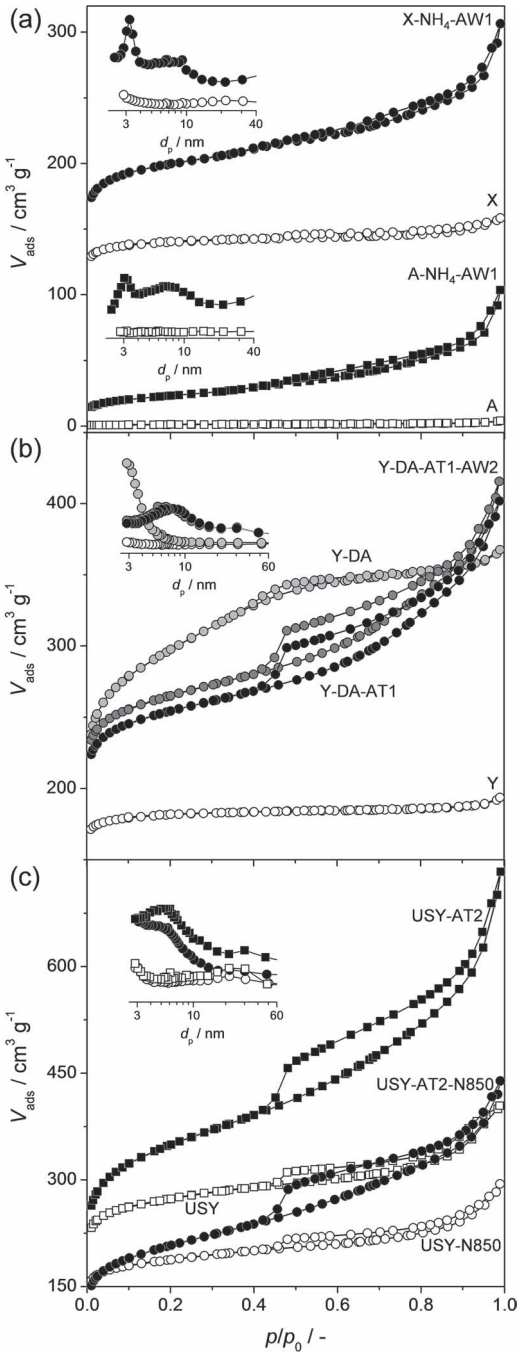

Figure 4. N_2 isotherms of conventional and hierarchical zeolites. a) X and A, b) Y, and c) USY zeolites. Insets: BJH mesopore size distributions.

in the yield or porosity resulted when the volume of NaOH solution per gram of zeolite was increased in attempts to enhance the dissolution (not shown). The low effectiveness of NaOH treatment for mesoporosity introduction is attributed to the simultaneous ion-exchange of the zeolite back to the more inert sodium form. A mild acid treatment using aqueous Na_2H_2EDTA (X-NH_4-AW2), an agent used in the removal of Al-rich debris from alkaline-treated Y zeolites,[16] was additionally employed. This treatment was not effective for the parent X, but it did enhance the dissolution (down to 83% yield) and induce limited mesopore formation (up to 43 $m^2\ g^{-1}$, Table 2) in the ammonium-exchanged zeolite X.

Unlike in the case of alkaline treatment, varying the volume of Na_2H_2EDTA solution (V_{EDTA}) proved more effective to improve the treatment efficiency. Raising V_{EDTA} from 15 to 90 $cm^3\ g^{-1}$ resulted in a linear decrease of the solid yields (down to 35%) and a concomitant linear increase of the external surface (S_{meso} up to 177 $m^2\ g^{-1}$, **Figure 5**a and Supporting Information Table S1). The efficiency of mesopore formation can be expressed by relating the amount of introduced external surface area to the associated weight loss.[31] In the case of the acid-treated X-NH_4-AW*x* samples, the relative external surface generated was ca. 2 $m^2\ g^{-1}$ per percent weight loss ($m^2\ g^{-1}\ \%^{-1}$). This is substantially lower than what was reported for alkaline-treated Y or USY zeolites, yielding values up to 8[16] and 12 $m^2\ g^{-1}\ \%^{-1}$,[17] respectively. Nevertheless, we expect that further optimization of these treatments will improve the efficiency. The solid treated with 60 $cm^3\ g^{-1}$ of solution (X-NH_4-AW1) combined a substantial external surface S_{meso} (122 $m^2\ g^{-1}$) with a fully preserved micropore volume (V_{micro} = 0.26 $cm^3\ g^{-1}$), and was accordingly selected for further characterization. Variation of the V_{EDTA} also enhanced dissolution and mesopore formation on treatment of the sodium-exchanged X zeolite, but to a much lower extent (Figure 5a). In addition, mesoporosity formation was even less efficient (Figure 5b).

The N_2 isotherm of sample X-NH_4-AW1 combined a preserved uptake at $p/p_0 < 0.1$, with a largely enhanced uptake at middle-to-high relative pressures (Figure 3a). The BJH mesopore size distribution revealed an enhanced uptake over the whole mesopore range, and a particularly pronounced contribution at 3 nm. High-resolution low-pressure Ar adsorption was performed to more precisely assess the influence of the treatments on the micropore region (Supporting Information Figure S1). The isotherms reveal that the uptake of X-NH_4-AW1 at low relative pressures was similar to that of the parent X zeolite, supporting the preservation of the intrinsic zeolitic properties. Transmission electron microscopy (TEM) demonstrated the significant impact of the treatments on the crystals' structure and morphology (Figure 2). Intracrystalline mesoporosity was clearly visible, which, unlike in the case of alkaline-treated zeolite Y,[16] was coupled with some intercrystalline mesoporosity. The presence of the intercrystalline mesoporosity is tentatively attributed to differences in the distribution of aluminum in the framework of zeolite X, which compared to zeolite Y,[32] was more prone to fragmentation upon chemical leaching.[33] TEM also provided further confirmation of the sample crystallinity, with lattice fringes, and sharp selected area electron diffraction patterns clearly observed (SAED, Figure 2). Scanning electron microscopy evidenced little change in the sample morphology, while the crystals appeared more eroded (Figure 3). ^{27}Al MAS NMR confirmed that the aluminum remained in tetrahedrally-coordinated framework positions after treatment (Supporting Information Figure S2). The Hg intrusion profile of zeolite X displayed a gradually increasing intrusion (0.2 $cm^3\ g^{-1}$) at low pressures (0.1–8 bar), a sharper intrusion of similar volume at 8 bar, and almost no intrusion at higher pressures (**Figure 6**a). The resulting pore size

Table 2. Treatment yields and properties of X and A zeolites.

Sample	Yield[a] [%]	Crystallinity[b] [%]	V_{micro}[c] [$cm^3\ g^{-1}$]	V_{meso}[d] [$cm^3\ g^{-1}$]	V_{pore}[e] [$cm^3\ g^{-1}$]	S_{meso}[c] [$m^2\ g^{-1}$]
X	–	100	0.23	0.03	0.26	22
X-AT1	100	95	0.23	0.06	0.29	26
X-AW2	98	99	0.27	0.04	0.31	31
X-NH_4	95	73	0.13	0.09	0.22	75
X-NH_4-AT1	90	–	0.26	0.08	0.34	53
X-NH_4-AW2	83	–	0.27	0.08	0.35	43
X-NH_4-AW1	52	56	0.26	0.19	0.45	122
X-Cs	–	–	0.21	0.02	0.23	15
X-NH_4-AW1-Cs	–	–	0.13	0.26	0.39	95
A	–	100	0	0	0	2
A-NH_4	98	95	0	0	0	3
A-NH_4-AW1	79	71	0.01	0.13	0.14	62
A-Cs	–	–	0	0	0	1
A-NH_4-AW1-Cs	–	–	0	0.12	0.12	59

[a]Grams of solid after treatment per gram of starting material; [b]XRD; [c]*t*-plot method; [d]$V_{meso} = V_{pore} - V_{micro}$; [e]Volume adsorbed at $p/p_0 = 0.99$.

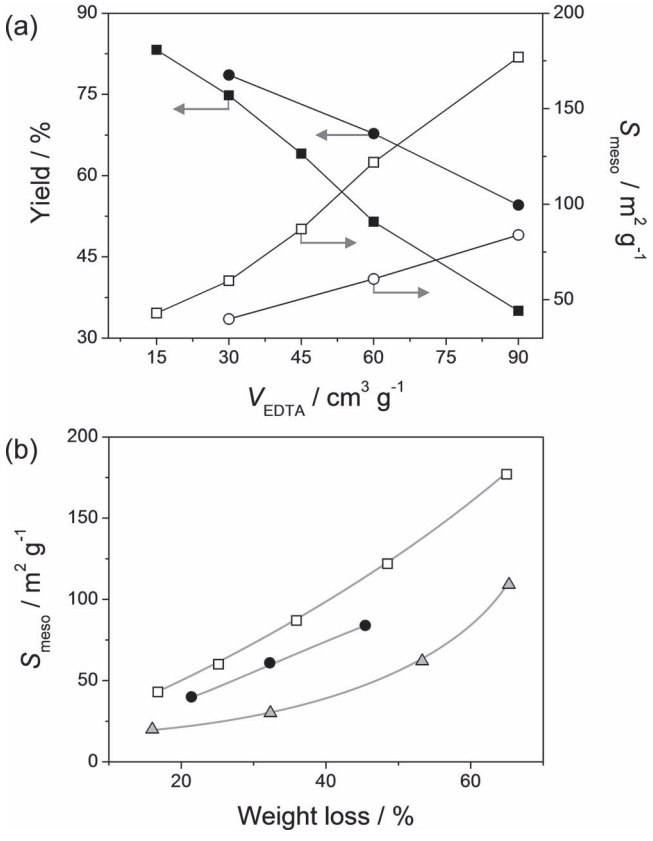

Figure 5. Relationship between the mesopore surface area (S_{meso}) and the yield of solids after Na_2H_2EDTA treatment. a) S_{meso} and yield as a function of the volume of Na_2H_2EDTA solution (0.11 M) per gram of zeolite (V_{EDTA}). b) S_{meso} as a function of the weight loss upon application of the acid treatments to X and A zeolites. Treatments were performed on "X', "X-NH_4", and "A-NH_4" zeolites, resulting in the "X-AW*x*" (circles), "X-NH_4-AW*x*" (squares), and "A-NH_4-AW*x*" (triangles) samples.

distribution revealed a single contribution centered at 1.5 µm, which is attributed to the intrusion into intercrystalline voids (Figure 6c). After treatment, the contribution between 0.1–8 bar pressure remained fairly similar, but the major intrusion, although of similar volume, occurred at a slightly higher pressure (10 bar). Correspondingly, the pore size distribution revealed a shift from 1.5 µm (X) to 1 µm in the treated zeolite. In line with the microscopic evidence, these observations point to a size reduction attributed to the fragmentation of some of the crystals during demetallation. Additionally, a marked intrusion of ca. 0.1 $cm^3\ g^{-1}$ occurred at pressures >400 bar, relating, in line with the N_2 adsorption results, to the presence of accessible mesopores.

Zeolite A: LTA-type zeolite A (Si/Al ratio ≈ 1.2) was subjected to the same experimental protocol developed for zeolite X. Treatments AT1 and AW2 proved similarly ineffective in developing hierarchical porosity in the parent NaA zeolite (data not shown). Again, after ion exchange of the zeolite from sodium to ammonium form, the Na_2H_2EDTA treatments substantially enhanced mesopore formation (Figure 5b, Table 2 and Supporting Information Table S1). The introduction of mesoporosity was slightly less efficient for zeolite A-NH_4 than for X-NH_4 (1.5 vs 2 $m^2\ g^{-1}\ \%^{-1}$, respectively). Moreover, unlike in the case of X, the increase of the S_{meso} as a function of weight loss followed an exponential trend. Such behavior was previously observed upon alkaline treatment of octadecasil.[34] In the latter case, the base leaching of the clathrasil framework resulted in the formation of purely intercrystalline mesoporosity. In the case of acid-treated zeolite A it remains difficult to quantitatively discriminate the relative contributions of intra- and intercrystalline mesoporosity. The nitrogen isotherm of A-NH_4-AW1 displayed a clearly enhanced uptake, amounting to a mesopore surface area of 62 $m^2\ g^{-1}$, that is, ca. 30 times that of the parent zeolite. In addition, the BJH mesopore size distribution showed, as in the case of X-NH_4-AW1, a sharp contribution at 3 nm. The presence of intra- and intercrystalline mesoporosity within the crystalline

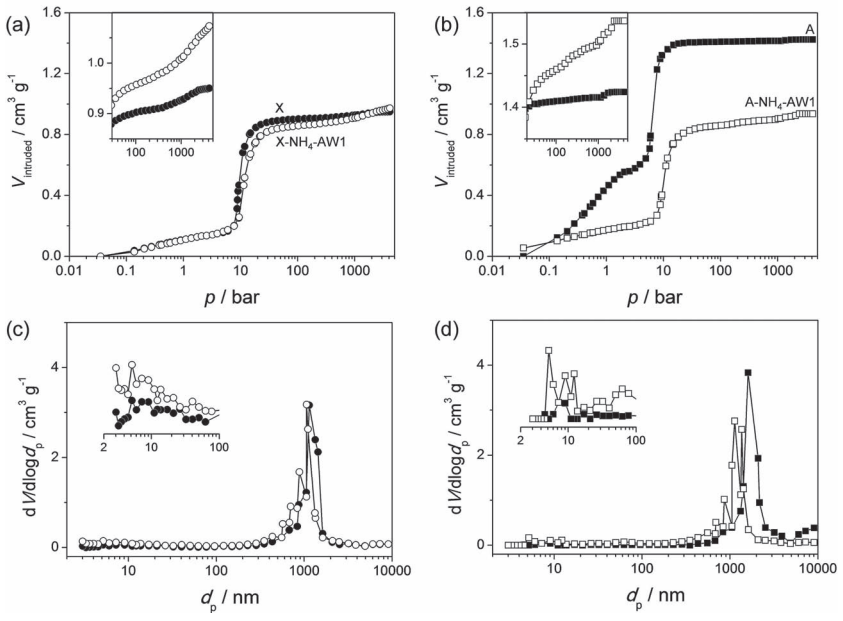

Figure 6. a,b) Hg intrusion curves and c,d) pore size distributions derived by the Washburn equation of conventional and hierarchical X and A zeolites. The insets in (a–d) highlight particular regions of each graph. For clearer visualization, the profiles of X-NH_4-AW1 and A-NH_4-AW1 are shifted upwards in the insets in (a) and (b) by 0.1 and 0.65 $cm^3\ g^{-1}$, respectively.

zeolite was again confirmed by TEM observation (Figure 2), while SEM showed that the crystal morphology and shape remained mostly intact, although the surface of the crystals appeared rougher (Figure 3). ^{27}Al MAS NMR confirmed that, like in the case for zeolite X, the bulk of the Al remained in framework positions (Figure S2). A sharp step around 10 bar was evidenced in the Hg intrusion curve of the parent A, corresponding to voids of ca. 2 μm in diameter (Figure 6b). Similarly to zeolite X, the post-synthetic modification led to a shift of the pore size distribution to smaller sizes (to ca. 1 μm). Additionally, in line with the N_2 adsorption results, an increased uptake at pressures >400 bar occurred, relating to the presence of accessible mesopores (inset Figure 6d). Hence, Na_2H_2EDTA treatment of the ammonium form represents a general strategy to introduce hierarchical porosity in low-silica zeolites. In effect, this result unlocks the full topological and compositional flexibility to prepare hierarchical zeolites by post-synthetic design.

Zeolite Y: Hierarchical Y zeolites were obtained following previously described post-synthetic modification strategies.[16] However, in this case the parent zeolite (Si/Al ≈ 2.5) was dealuminated using a controlled (rather than direct) addition of H_4EDTA, resulting in a highly crystalline zeolite Y-DA (Si/Al ratio = 5.4, Figure 1, **Table 3**). The presence of small (2–3 nm) mesopores was clearly evidenced in TEM images (**Figure 7**) and in the mesopore size distribution (Figure 4b) of Y-DA. The large resulting mesopore surface area (S_{meso} = 388 $m^2\ g^{-1}$) demonstrated that highly mesoporous zeolites can be obtained upon dealumination by controlled acid leaching. In accordance with previous observations,[16] the microporosity, crystallinity, as well as the mesopore size, increased after alkaline (Y-DA-AT1) and subsequent acid (Y-DA-AT1-AW2) treatments. Since the mesopore volume of the treated Y zeolites remained mostly constant, the total surface area decreased with increasing mesopore size (Table 3). ^{27}Al MAS NMR experiments confirmed that all of the aluminum in the starting and hierarchical Y zeolites was located in the framework (Supporting Information Figure S3).

Table 3. Properties of Y and USY zeolites.

Sample	Crystallinity[a] [%]	Si/Al[b] [mol mol^{-1}]	Cs content[c] [wt%]	Cs/Al [mol mol^{-1}]	V_{micro}[d] [$cm^3\ g^{-1}$]	V_{meso}[e] [$cm^3\ g^{-1}$]	V_{pore}[f] [$cm^3\ g^{-1}$]	S_{meso}[d] [$m^2\ g^{-1}$]	ρ_s[g] [$g\ cm^{-3}$]	Basicity[h] [%]
Y	100	–	–	–	0.27	0.03	0.30	28	2.08	–
Y-DA	78	–	–	–	0.29	0.27	0.56	388	2.05	–
Y-DA-AT1	97	–	–	–	0.33	0.30	0.63	180	2.23	–
Y-DA-AT1-AW2	93	–	–	–	0.32	0.28	0.60	168	2.24	–
Y-Cs	29	2.7	0.20	0.56	0.24	0.01	0.25	6	2.19	100
Y-DA-Cs	32	5.4	0.17	0.71	0.19	0.17	0.36	229	2.18	41
Y-DA-AT1-Cs	34	3.8	0.19	0.61	0.22	0.20	0.42	122	2.27	66
Y-DA-AT1-AW2-Cs	35	4.2	0.18	0.62	0.24	0.23	0.47	132	2.54	77
USY	100	–	–	–	0.32	0.30	0.62	227	–	–
USY-AT2	98	–	–	–	0.28	0.77	1.05	523	–	–
USY-Cs	–	17	0.06	0.52	0.25	0.24	0.49	179	–	22
USY-AT2-Cs	–	11	0.11	0.61	0.22	0.57	0.79	428	–	35

[a]XRD; [b]ICP-OES; [c]AAS; [d]*t*-plot method; [e]$V_{meso} = V_{pore} - V_{micro}$; [f]Volume adsorbed at $p/p_0 = 0.99$; [g]He pycnometry; [h]Integral of the CO_2-TPD profile, relative to sample Y-Cs.

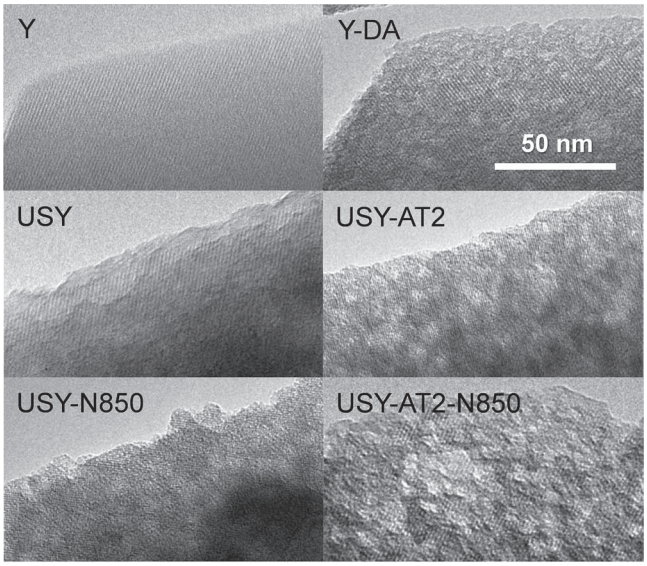

Figure 7. Transmission electron micrographs of conventional and hierarchical Y and USY zeolites. The scale bar applies to all images.

Zeolite USY: The USY zeolite investigated in this study had a nominal Si/Al ratio of 15.[35] The hierarchical analogue of this zeolite was obtained by treatment in an aqueous solution of tetrapropylammonium (TPA^+) bromide (0.2 M) and NaOH (0.3 M). During this treatment TPA^+ acts as a pore directing agent (PDA), enabling the introduction of mesoporosity while preventing amorphization of the crystal structure.[17] Compared to previous work,[17] the USY zeolite was treated using a higher alkalinity (0.3 M NaOH) to enhance mesopore formation. The resulting solid (USY-AT2) displayed the archetypical N_2 isotherm of a hierarchical USY zeolite (Figure 4c), and combined a mesopore surface area of over 500 $m^2\ g^{-1}$ with a largely preserved crystallinity and microporosity (Table 3). The Si/Al ratio decreased from 17 to 11. The influence of the introduction of mesoporosity in the USY zeolites was studied in more detail by DRIFTS in the hydroxyl stretching region and ^{27}Al MAS NMR. The spectrum of the parent USY zeolite comprised three bands, attributed to the isolated external silanols (3739 cm^{-1}) and Brønsted acidic hydroxyls (3624 and 3561 cm^{-1}), respectively (**Figure 8**). In agreement with previous work,[17] these three bands appeared more intense following alkaline treatment in the presence of TPA^+. The intensity of the band at 3739 cm^{-1} increased due to the larger external surface area. Moreover, the Brønsted hydroxyl stretching bands became more intense due to the removal of amorphous Si-rich debris residual from steaming and dealumination treatments applied during the preparation of the commercial sample. The ^{27}Al MAS NMR spectra of USY and USY-AT2 reveal that the majority of Al remained in the framework upon post-synthetic modification (Supporting Information Figure S3).

2.2. Basicity Introduction

Nitridation: The incorporation of nitrogen into the zeolite framework was performed in a continuous-flow fixed-bed reactor by high-temperature nitridation in an ammonia mixture. This treatment forms amido or imido species that display a distinct basicity.[36] Nitridation was performed on a USY zeolite with Si/Al ≈ 15 since, in comparison with zeolite Y, it is relatively stable upon treatment. To avoid an excessive pressure drop in the reactor, the zeolite powders were sieved into 200–400-µm fractions before treatments. The whole sieving procedure, involving pressing, crushing, and sieving, caused a reduction in porous properties of the resulting samples (USY-SF and USY-AT2-SF, Supporting Information Table S2). The micropore volume reduced by 22% (USY-SF) and 18% (USY-AT2-SF), while the mesoporous surface area decreased by 16% (USY-SF) and 25% (USY-AT2-SF). The influence of nitridation on the crystallinity, nitrogen content, and porosity of the treated zeolites is depicted in **Figure 9**. The nitrogen content increased (up to ca. 7 wt%) with treatment temperature for both samples. Interestingly, the mesoporous zeolite incorporated less nitrogen than the parent zeolite at lower temperatures, whereas this trend was reversed at temperatures ≥750 °C. The parent zeolite was largely unaffected by the treatments in terms of crystallinity and porosity. The hierarchical zeolite, however, proved somewhat less stable. Sample USY-AT2 displayed a reduction of ca. 60% in crystallinity, independent of the reaction temperature. The external surface decreased from 388 to below 200 $m^2\ g^{-1}$ (after treatment at 950 °C), while the micropore volume decreased from 0.23 down to 0.06 $cm^3\ g^{-1}$. TEM and N_2 sorption confirmed that, after nitridation at 850 °C, the sample structure, morphology, and porosity remained mostly intact for both the conventional and hierarchical zeolites (Figures 4 and 7).

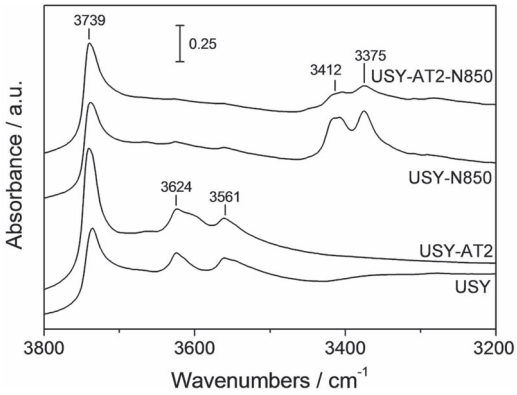

Figure 8. Infrared spectra in the OH stretching region of USY zeolites.

The influence of the nitridation treatment was studied in more detail by FTIR and ^{27}Al MAS NMR for samples USY-N850 and USY-AT2-N850. The OH stretching region in the FTIR spectra showed that the band related to isolated surface silanols (3739 cm^{-1}) remained similar for the parent zeolite upon nitridation (Figure 8). However, the latter band decreased in intensity for USY-AT2-N850, which is in line with the decreased external surface area. The bands associated with Brønsted acid sites (3624 and 3561 cm^{-1}) were barely distinguishable in either nitrided sample. Instead, the presence of two bands at 3412 and 3375 cm^{-1} evidenced the transformation of Brønsted acid groups into predominantly imido groups.[36] The similar appearance of these bands suggests that the basic sites introduced in samples USY-N850 and USY-AT2-N850 are comparable. Nevertheless,

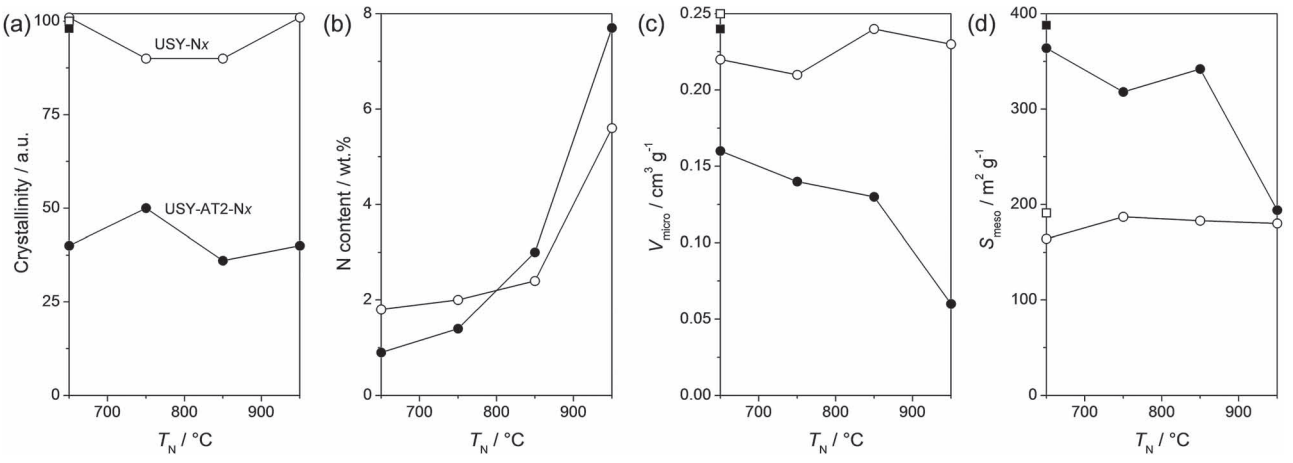

Figure 9. Influence of the nitridation temperature (T_N) on the a) crystallinity, b) nitrogen content, c) micropore volume, and d) mesopore surface area of conventional (open circles) and hierarchical (solid circles) USY zeolites. The properties of USY-SF and USY-AT2-SF are represented by the open and solid squares, respectively.

the bands at 3412 and 3375 cm^{-1} appeared broader and less intense for the mesoporous sample. The latter could be due to a larger degree of thermal dehydroxylation during treatment of this sample.[36] ^{27}Al MAS NMR evidenced the disappearance of the bands at 0 ppm, related to octahedrally coordinated extra-framework aluminum, upon nitridation. In addition, the band at 59 ppm due to framework aluminum was significantly broadened (Supporting Information Figure S3).

Cesium Exchange: Lattice oxygen atoms, bearing a partial negative charge, give rise to a Lewis-type basicity in the framework of alkali-exchanged zeolites. The activity of such basic zeolites was reported to increase with higher framework Al content (higher cation exchange capacity) and increasing countercation radius, following the trend $Cs^+ > Rb^+ > K^+ > Na^+ > Li^+$.[24,37,38] In this work, we have therefore focused on cesium-exchanged zeolites.

Cesium exchange was performed on conventional and hierarchical A, X, Y, and USY zeolites (Tables 2 and 3). Based on the catalytic performance (vide infra), further study of the Cs-exchanged zeolites focused on zeolite Y. After cesium exchange, the apparent crystallinity of the Y zeolites decreased by ca. two thirds (Figure 1), based on the high electron density associated with Cs-exchanged zeolites.[27,27] Al MAS NMR confirmed that all aluminum remained in framework positions (Supporting Information Figure S3). The porosity of each zeolite reduced after incorporation of Cs into the solid. This is attributed to the increased skeletal densities (Table 3), and the relatively large volume that the Cs^+ cations occupy within the zeolite structure.[27] Independent of the Al content, all hierarchical analogues comprised a higher molar Cs/Al ratio than the conventional starting zeolites (Table 3). This enhanced degree of ion exchange is attributed to the increased accessibility of the exchange sites facilitated by the external surface area. It should be emphasized that the Cs/Al ratio is based on bulk values, and does not discriminate on the nature of the aluminum. For example, base leaching typically results into the extraction of both Si and Al from the solid, but aluminum species can be redeposited on the solid in the form of "realuminated" species.[39] These species, although displaying particular acidity,[40] are not considered as classical framework aluminum and their cation exchange capacity remains unclear.

The basicity of the Cs-exchanged zeolites was evaluated by CO_2-TPD (**Figure 10**). The CO_2 desorption profiles evidenced a substantially larger concentration and a higher strength of basic sites in Y zeolites compared to the USY zeolites. The post-synthetic modifications of the Y zeolites did not affect the basic strength as demonstrated by the similar temperature of the desorption peak. They did invoke a reduction in basicity, which relates well with the evaluation of the Si/Al ratios (Table 3). Nevertheless, whereas Y-DA-AT1-Cs displays a lower Si/Al ratio, and higher Al content than Y-DA-AT1-AW2-Cs, its total basicity was lower. This difference is attributed to the presence of realuminated species in Y-DA-AT1-Cs, which are unable to give rise to the same CEC as fully-coordinated framework aluminum. In the case of the USY zeolites, the total basicity increased slightly after treatment which could be explained by the higher Al content. However, taking the apparently lower CEC of realuminated species into account, the increased basicity was attributed to the removal of amorphous Si-rich species present in the as-received USY zeolite.[17]

2.3. Catalytic Evaluation

The condensation of benzaldehyde with malononitrile (**Scheme 1**) was selected as a model base-catalyzed reaction to evaluate the performance of the conventional and hierarchical zeolites.[41] The conversion of benzaldehyde (X_{BA}) was taken as a measure of the catalytic activity. In general, all catalytic tests resulted in selectivities of >90% to benzylidenemalononitrile, the desired product. This implies that the enhanced secondary porosity did not alter the reaction selectivity. Reactions were performed at 25, 50, or 80 °C, temperatures at which minimal conversion occurs in the absence of a catalyst (**Figure 11**a). Furthermore, no apparent conversion was evidenced over the protonic form of USY under these conditions.

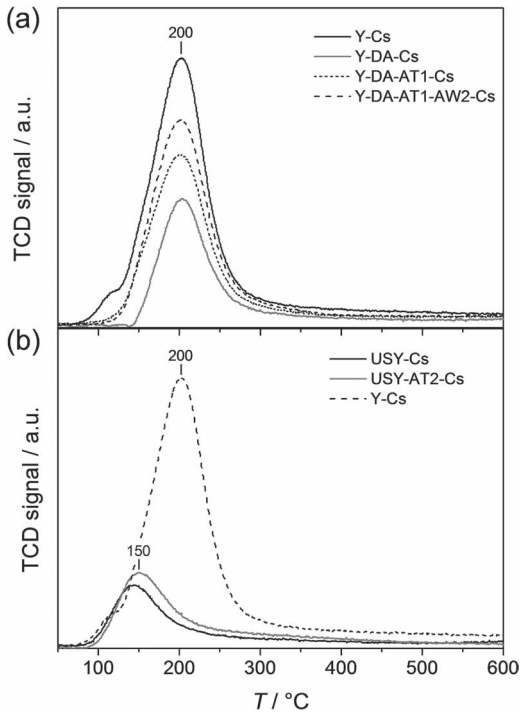

Figure 10. CO_2-TPD profiles of conventional and hierarchical Y and USY zeolites.

Nitrided Zeolites: Application of the nitrided USY zeolite catalysts invoked substantially increased conversions (Figure 11a). Sample USY-N850 displayed a conversion of ca. 25% after 4 h, while the hierarchical sample USY-AT2-N850 was about twice as active. A more complete picture was obtained by evaluating the catalytic performance of the parent and hierarchical USY zeolites nitrided at different temperatures ("T_N", Figure 11b). At T_N = 650 °C, the conventional zeolite outperforms the hierarchical zeolite, which can be attributed to the lower nitrogen content in the mesoporous zeolite. However, at 750 and 850 °C, where the nitrogen contents are roughly similar, the mesoporous zeolites exhibited superior catalytic performance. The latter was particularly evident in the case of nitridation at 750 °C. After T_N = 950 °C, despite having a higher nitrogen content, the hierarchical zeolite displayed a similar catalytic performance to the conventional zeolite, which is attributed to the comparable mesoporosity of these samples. The Knoevenagel condensation was performed at different temperatures (T_K) using samples USY-N850 and USY-AT2-N850 in order to estimate the activation energy (Figure 11c). The resulting values were in both cases ca. 36 kJ mol^{-1}, indicating that the active sites are not altered by the post-synthetic modifications.

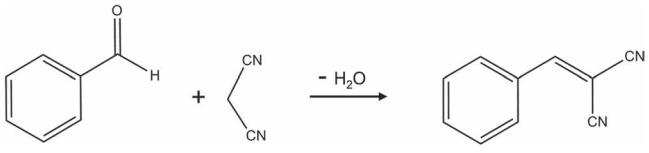

Scheme 1. Knoevenagel condensation of benzaldehyde with malononitrile.

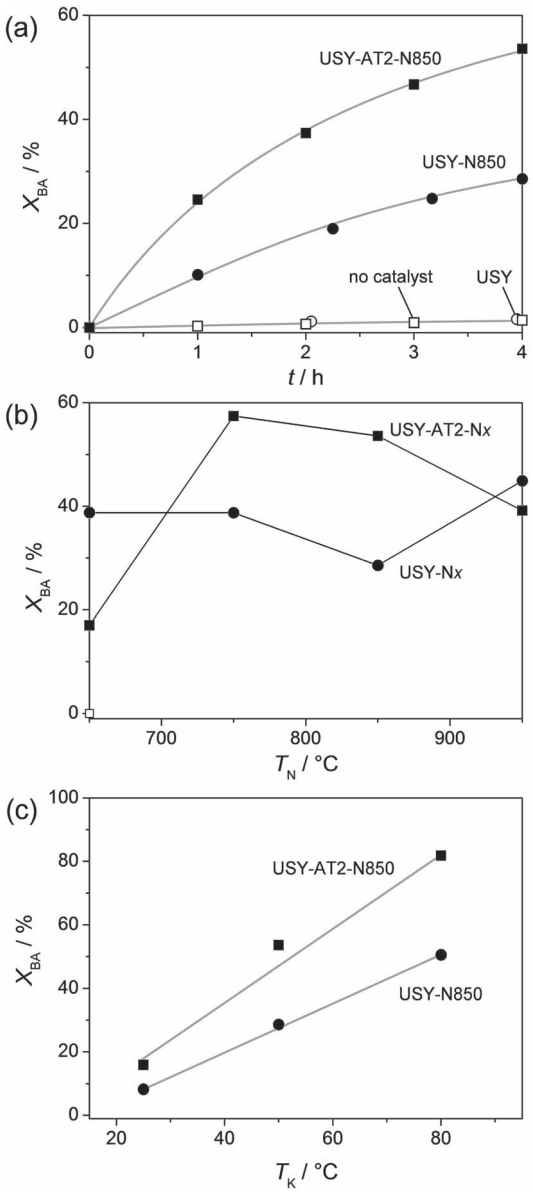

Figure 11. Catalytic evaluation of USY zeolites in the Knoevenagel condensation of benzaldehyde with malononitrile. a) Conversion of benzaldehyde (X_{BA}) as a function of time at 50 °C, b) X_{BA} after t = 4 h at 50 °C as a function of nitridation temperature (T_N), c) X_{BA} at t = 4 h as a function of the Knoevenagel reaction temperature (T_K).

Cesium-Exchanged Zeolites: The performance of the Cs-exchanged zeolites is shown in **Figure 12**a. The conventional Y-Cs displayed a limited conversion of benzaldehyde (X_{BA} < 5%). Conversely, the dealuminated sample (Y-DA-Cs), comprising less than half the basicity of Y-Cs, displayed a 10 times higher conversion (X_{BA} = 50%). Sample Y-DA-AT1-Cs displayed a conversion of 30%, whereas the washed sample (Y-DA-AT1-AW2-Cs) evidenced an X_{BA} of 50%. Taking the comparable porosities of Y-DA-AT1-AW2-Cs and Y-DA-AT1-Cs into account, the 20% difference in activity clearly illustrates the beneficial impact of the acid wash. On the other hand, the similar performance of

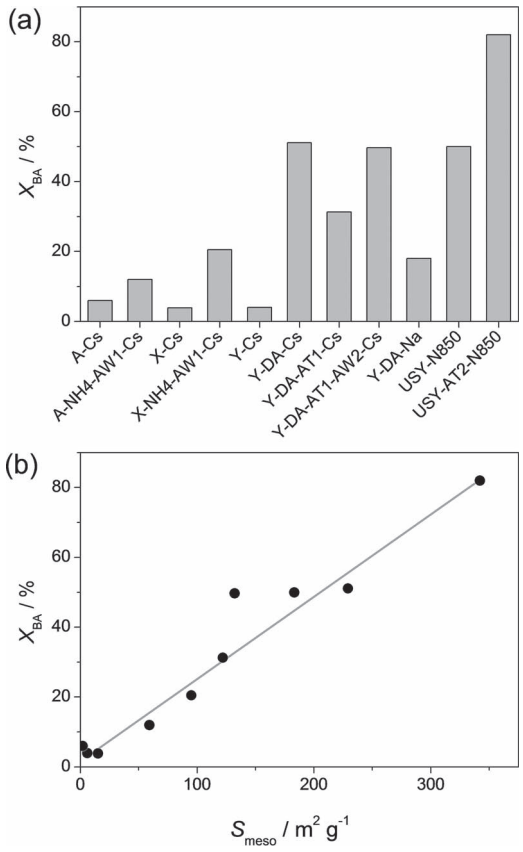

Figure 12. a) Catalytic evaluation of FAU and LTA-type zeolites in the Knoevenagel condensation of benzaldehyde with malononitrile at 80 °C and t = 4 h. b) The conversion of benzaldehyde (X_{BA}) as a function of the mesopore surface (S_{meso}) for the Cs-exchanged and nitrided zeolites in (a).

Y-DA-Cs and Y-DA-AT1-AW2-Cs suggests that the mesopore size has a negligible influence. The latter makes sense since the kinetic diameter of the product (ca. 1 nm) is substantially smaller than the 2–3 nm diameter of the mesopores. The sodium form of the dealuminated Y zeolite (Y-DA-Na) displayed a conversion of 20%, i.e., less than half the activity than that of the cesium form. Nevertheless, the performance remains ca. 5 times higher than the conventional Y-Cs zeolite, which is of particular environmental and commercial interest. Zeolite X-Cs and A-Cs performed similarly to Y-Cs, that is, $X_{BA} \leq 5\%$. As observed for the Y zeolites, the introduction of mesoporosity in zeolite X and A resulted in an increased conversion (X_{BA} = 20% for X-NH_4-AW1-Cs and X_{BA} = 12% for A-NH_4-AW1-Cs). The relatively small catalytic enhancement is attributed to the lower degree of mesoporosity in the hierarchical X and A zeolites compared to zeolite Y.

Compared to the nitrided samples USY-N850 and USY-AT2-N850, the Cs-exchanged zeolites were less active (Figure 12a). Nonetheless, the relative gain in activity, on application of the hierarchical variant, greatly exceeded that observed for the nitrided samples; whereas the latter displayed a doubled conversion, the Cs-exchanged samples were up to 10 times more active. The relatively large activity gain for X and Y zeolites is attributed to the very low external surface area of the parent X and Y zeolites (ca. 20 m^2 g^{-1}), being an order of magnitude lower than that of USY (227 m^2 g^{-1}). To evaluate the role of the secondary porosity in greater detail, the activities of the Cs-containing and nitrided zeolites were plotted against S_{meso} (Figure 12b). The resulting linear trend suggests, in line with the similar activation energies (vide supra), that the external surface plays a dominant role in determining the catalytic conversions. This point is further supported by the fact that the linear relationship also holds for the A zeolites. After all, the LTA micropores are ca. 0.4 nm in size, inferring that the reaction can only occur at the external surface. Strikingly, in Knoevenagel condensations on alkali-exchanged zeolites, the reaction rate was reported to be unaffected by the size, hence external surface, of the zeolites.[37] However, that conclusion was based on catalytic tests performed on zeolites of average sizes 0.8 and 0.47 μm. Assuming a density of 2.2 g cm^{-3}, the external surfaces of these crystals can be calculated to be in the range of 2–5 m^2 g^{-1}, which is unparalleled to those reported in this contribution (>100 m^2 g^{-1}).

The pronounced role of the external surface area in base catalysis has pervasive implications. First and foremost, our results demonstrate that reactions catalyzed by basic zeolites suffer from significant transport and/or access limitations. The possibility to transform any zeolite into a hierarchical form enables to overcome these difficulties, revitalizing the use of zeolites as base catalysts, particularly in reactions where the size of the reagents, let alone that of the products, exceeds the micropore size. Examples hereof are commonly encountered in the synthesis of fine chemicals as fragrances and dyes.[42] With such large molecular sizes, it is conceivable, that the size and uniformity of the mesopores is also important, e.g., by giving rise to a mesopore-induced shape selectivity.[43] Additionally, it is possible that certain zeolites, i.e., those assumed not to possess the required basic strength for a particular reaction, become viable catalysts based on the introduced secondary porosity. Finally, we anticipate that the improved accessibility of the micropore structure may enhance the efficiency of other base modifications, like the intrazeolitic deposition of metal clusters[26] and oxides[27] or the use of alkylammonium cations.[44]

3. Conclusions

By combining recently established post-synthetic treatments, with a novel route for Al-rich (Si/Al ≈ 1) zeolites, hierarchical A, X, Y, and USY zeolites were prepared and subsequently converted into basic catalysts by nitridation or alkali ion exchange. In both cases, the presence of the secondary porous network facilitated an enhanced incorporation of either nitrogen or cesium in the solids. Catalytic evaluation of the basic hierarchical zeolites in the Knoevenagel condensation of benzaldehyde with malononitrile demonstrated that the secondary porosity plays a vital role, attaining activities up to 10 times higher than the conventional zeolites. For Cs-exchanged zeolites, the role of the external surface largely exceeded that of the total basicity. Our results underline the prospects of hierarchical zeolites in base catalysis, particularly in the conversion of bulky substrates, such as those often encountered in the manufacture of fine chemicals.

4. Experimental Section

Materials and Procedures: The X and A zeolites (sodium form, Si/Al ≈ 1.2, coded "X" and "A", respectively) were provided by Acros. The Y zeolite (ammonium form, CBV300, Si/Al = 2.6, coded "Y") and the steamed and dealuminated USY zeolite (protonic form, CBV720, Si/Al = 15, coded "USY") were provided by Zeolyst International.

Post-synthetic modifications were undertaken using the aqueous solutions and conditions reported in Table 1. Treatments involving volumes of up to 100 cm^3 were performed under magnetic stirring using an Easymax 102 instrument from Mettler Toledo. Treatments involving solutions of 100–500 cm^3 were executed under magnetic stirring in a round-bottomed flask equipped with a reflux condenser. The controlled addition of H_4EDTA was achieved using a Soxhlet reactor. In a typical experiment, the zeolite sample (0.3–100 g) was added to a vigorously stirred solution of the desired solute, molarity (0.1–3 M), and temperature (25–100 °C), and was left to react for the required time (0.5–72 h). Afterwards, the reaction was quenched and the resulting solid was filtered, washed using distilled water, and dried overnight at 65 °C. In the case TPABr was included in the alkaline solution, the obtained powder was calcined in air at 550 °C for 5 h, using a heating rate of 5 °C min^{-1}. Acid treatments using Na_2H_2EDTA were labeled "AW*x*" (AW: acid wash), while the treatment aimed at framework dealumination was labeled "DA". Alkaline treatments (in the presence or absence of TPABr) were labeled "AT*x*". The suffix "*x*" represents integers for further specification. After ion exchange of the zeolites to the ammonium, sodium, or cesium form, the codes "NH_4", "Na", or "Cs" were used, respectively.

Prior to nitridation, sieve fractions (200–400 μm, code "SF") were prepared by pressing the powder (ca. 1 g) using 8 tons of pressure for several minutes, crushing the resulting pellets, and sieving. Nitridation was performed on the sieve fraction (0.5 g) placed in a quartz tubular fixed-bed reactor. The sample was heated to the desired reaction temperature (650–950 °C) at a ramp rate of 10 °C min^{-1} in 10vol% NH_3 in He (30 cm^3 min^{-1}). This reaction was continued using the same flow and temperature for 48 h. After reaction, the reactor was cooled to room temperature in a helium flow, and the resulting solids were stored under a nitrogen atmosphere. Sieved and nitrided zeolites were labeled "N*x*", where "*x*" represents the reaction temperature.

Characterization: Powder X-ray diffraction (XRD) patterns were acquired with a PANanalytical X'Pert PRO-MPD diffractometer in Bragg–Brentano geometry using Ni-filtered Cu Kα radiation (λ = 0.1541 nm). Data were recorded in the 2θ range of 3–60° with an angular step size of 0.05° and a counting time of 8 s per step. The relative crystallinity of the faujasite samples was determined according to the method described by the American Society for Testing and Materials (ASTM), standard D3906. Similarly, for zeolite A, the method described in standard D5357 was followed. Si and Al concentrations in the solids were determined by inductively coupled plasma optical emission spectroscopy (ICP-OES) on a Horiba Ultima 2 instrument equipped with photomultiplier tube detection. Cs concentrations were determined by atomic absorption spectroscopy (AAS) using a Varian SpectrAA 220 FS instrument, while N concentrations were analyzed using using a LECO CHN-900 combustion furnace. Transmission electron microscopy (TEM) and selected area electron diffraction (SAED) measurements were performed using a FEI Tecnai F30 microscope operated at 300 kV or a Phillips CM12 instrument operated at 100 kV. Scanning electron microscopy (SEM) was carried out on a Zeiss Gemini 1530 FEG microscope operated at 5 kV. Nitrogen sorption at −196 °C was carried out in a Micromeritics TriStar II instrument. Prior to the measurement, the samples were degassed in vacuum at 300 °C for 3 h. The *t*-plot method was used to discriminate between micro- and mesoporosity. The mesopore size distribution was obtained by the Barrett–Joyner–Halenda (BJH) model applied to the adsorption branch of the isotherm. High-resolution low-pressure Ar adsorption isotherms were recorded at −196 °C on a Micromeritics ASAP 2020 analyzer after evacuation at 300 °C for 8 h. The hybrid nonlinear density functional theory (NLDFT) model describing argon adsorption in cylindrical micro- and mesopores was used to calculate the pore size distribution. Mercury intrusion porosimetry was performed in the pressure range from vacuum to 4000 bar on a Micromeritics Autopore IV 9510. Degassing was undertaken in situ. A contact angle of 140 ° for mercury and the Washburn equation were used to derive the corresponding pore size distribution. The skeletal density of the solids was measured by He pycnometry performed on a Micromeritics Accupyc II 1340 instrument. Prior to analysis, the samples (ca. 0.3 g) were dried in vacuum at 100 °C for 4 h. The density was obtained by taking the average of 50 measurements after equilibration for 150 measurements. Temperature-programmed desorption of CO_2 (CO_2-TPD) was carried out in a Thermo TPDRO 1100 unit equipped with a thermal conductivity detector. The zeolite (0.1 g) was pre-treated at 550 °C in He flow (30 cm^3 min^{-1}) for 3 h. Afterwards, 2 vol% of CO_2 in N_2 (30 cm^3 min^{-1}) was adsorbed at 50 °C for 90 min, followed by He purging at the same temperature for 60 min. Finally, desorption of CO_2 was monitored in the range of 50–700 °C (heating rate: 10 °C min^{-1}). Fourier transform infrared (FTIR) spectroscopy was carried out in a Thermo Nicolet 5700 spectrometer equipped with a SpectraTech Collector II diffuse reflectance (DRIFTS) accessory and a high-temperature cell. Prior to the measurement, the samples were dried at 300 °C in flowing N_2 (100 cm^3 min^{-1}) for 60 min. Spectra were recorded under a N_2 atmosphere at 200 °C, in the range of 650–4000 cm^{-1}, by co-addition of 200 scans and with a nominal resolution of 4 cm^{-1}.[27] Al magic angle spinning nuclear magnetic resonance (MAS NMR) spectroscopy was performed at a spinning speed of 10 kHz on a Bruker Avance 400 spectrometer equipped with a 4 mm probe head and 4 mm ZrO_2 rotors at 182.4 MHz. Spectra were obtained using 2048 accumulations, 90° pulses with a pulse length of 2.4 μs, a recycle delay of 0.25 s, and with $(NH_4)Al(SO_4)_2{\cdot}12\ H_2O$ as a reference.

Catalytic Testing: The Knoevenagel condensation of malononitrile with benzaldehyde was carried out in a three-necked round-bottom flask equipped with a reflux condenser under vigorous magnetic stirring. Experiments were performed under N_2 atmosphere to prevent oxidation of benzaldehyde. In a typical experiment, malononitrile (4 mmol), benzaldehyde (4 mmol), and *n*-decane (5 mmol, used as internal standard), were added to 30 cm^3 of toluene, and heated to the desired temperature (30, 50, or 80 °C). Afterwards, the catalyst (0.05 g) was added, followed by time-resolved sampling. The products were analyzed off-line using an HP Agilent 6890 gas chromatograph equipped with a 25 m CPSIL8CB column and FID detector.

Supporting Information

Supporting Information is available from the Wiley Online Library or from the author.

Acknowledgements

The Swiss National Science Foundation (project number 200021-134572) is acknowledged. The Electron Microscopy Centre of the Swiss Federal Institute of Technology (EMEZ) is acknowledged for use of their facilities. This article was modified after online publication. The concentrations in the description of the catalytic tests in the Experimental Section were corrected.

Received: August 14, 2012
Revised: October 18, 2012
Published online: November 7, 2012

[1] A. Corma, *Chem. Rev.* **1995**, *95*, 559.
[2] W. Vermeiren, J.-P. Gilson, *Top. Catal.* **2009**, *52*, 1131.
[3] J. Pérez-Ramírez, C. H. Christensen, K. Egeblad, C. H. Christensen, J. C. Groen, *Chem. Soc. Rev.* **2008**, *37*, 2530.
[4] R. Chal, C. Gérardin, M. Bulut, S. van Donk, *ChemCatChem* **2011**, *3*, 67.

[5] S. Lopez-Orozco, A. Inayat, A. Schwab, T. Selvam, W. Schwieger, *Adv. Mater.* **2011**, *23*, 2602.
[6] J. Pérez-Ramírez, *Nat. Chem.* **2012**, *4*, 250.
[7] A. Corma, M. J. Díaz-Cabañas, J. L. Jordá, C. Martínez, M. Moliner, *Nature* **2006**, *443*, 842.
[8] E.-P. Ng, D. Chateigner, T. Bein, V. Valtchev, S. Mintova, *Science* **2012**, *335*, 70.
[9] W. J. Roth, J. Čejka, *Catal. Sci. Technol.* **2011**, *1*, 43.
[10] A. Corma, V. Fornes, S. B. Pergher, T. L. M. Maesen, J. G. Buglass, *Nature* **1998**, *396*, 353.
[11] M. Choi, K. Na, J. Kim, Y. Sakamoto, O. Terasaki, R. Ryoo, *Nature* **2009**, *461*, 246.
[12] K. Egeblad, C. H. Christensen, M. Kustova, C. H. Christensen, *Chem. Mater.* **2008**, *20*, 946.
[13] D. Verboekend, J. Pérez-Ramírez, *Catal. Sci. Technol.* **2011**, *1*, 879.
[14] F. Thibault-Starzyk, I. Stan, S. Abelló, A. Bonilla, K. Thomas, C. Fernandez, J.-P. Gilson, J. Pérez-Ramírez, *J. Catal.* **2009**, *264*, 11.
[15] D. Verboekend, K. Thomas, M. Milina, S. Mitchell, J. Pérez-Ramírez, J.-P. Gilson, *Catal. Sci. Technol.* **2011**, *1*, 1331.
[16] D. Verboekend, G. Vilé, J. Pérez-Ramírez, *Adv. Funct. Mater.* **2012**, *22*, 916.
[17] D. Verboekend, G. Vilé, J. Pérez-Ramírez, *Cryst. Growth Des.* **2012**, *12*, 3123.
[18] M. Choi, H. S. Cho, R. Srivastava, C. Venkatesan, D. H. Choi, R. Ryoo, *Nat. Mater.* **2006**, *5*, 718.
[19] A. Inayat, I. Knoke, E. Spiecker, W. Schwieger, *Angew. Chem. Int. Ed.* **2012**, *51*, 1962.
[20] E. M. Flanigen, R. W. Broach, S. T. Wilson, in *Zeolites in Industrial Separation and Catalysis* (Ed. S. Kulprathipanja), **2010**, Wiley-VCH, Weinheim, Germany, pp. 1–17.
[21] M. S. Holm, E. Taarning, K. Egeblad, C. H. Christensen, *Catal. Today* **2011**, *168*, 3.
[22] G. V. Shanbhag, M. Choi, J. Kim, R. Ryoo, *J. Catal.* **2009**, *264*, 88.
[23] H. Hattori, *Chem. Rev.* **1995**, *95*, 537.
[24] J. Weitkamp, M. Hunger, U. Rymsa, *Microporous Mesoporous Mater.* **2001**, *48*, 255.
[25] Y. Ono, *J. Catal.* **2003**, *216*, 406.
[26] L. R. M. Martens, P. J. Grobet, P. A. Jabobs, *Nature* **1985**, *315*, 568.
[27] P. Hathaway, M. E. Davis, *J. Catal.* **1989**, *116*, 263.
[28] S. Ernst, M. Hartmann, S. Sauerbeck, T. Bongers, *Appl. Catal., A* **2000**, *200*, 117.
[29] H. K. Beyer, in *Molecular Sieves*, Vol. *3* (Eds: H. G. Karge, J. Weitkamp), **2002**, Springer, Berlin, p. 232.
[30] G. H. Kühl, A. E. Schweizer, *J. Catal.* **1975**, *38*, 469.
[31] D. Verboekend, A. M. Chabaneix, K. Thomas, J.-P. Gilson, J. Pérez-Ramírez, *CrystEngComm* **2011**, *13*, 3408.
[32] S. Ramdas, J. M. Thomas, J. Klinowski, C. A. Fyfe, J. S. Hartman, *Nature* **1981**, *292*, 228.
[33] R. L. Hartman, H. S. Fogler, *Langmuir* **2007**, *23*, 5477.
[34] J. Pérez-Ramírez, S. Abelló, L. A. Villaescusa, A. Bonilla, *Angew. Chem. Int. Ed.* **2008**, *120*, 8031.
[35] http://www.zeolyst.com/our-products/standard-zeolite-powders/zeolite-y.aspx (accessed October 2012).
[36] M. Srasra, S. Delsarte, E. M. Gaigneaux, *J. Phys. Chem. C* **2010**, *114*, 4527.
[37] A. Corma, V. Fornés, R. M. Martín-Aranda, H. Garcia, J. Primo, *Appl. Catal.* **1990**, *59*, 237.
[38] A. Corma, S. Iborra, in: *Fine Chemicals through Heterogeneous Catalysis* (Eds. R. A. Sheldon, H. van Bekkum), **2001**, Wiley-VCH, Weinheim, Germany., pp. 313–317.
[39] D. Verboekend, S. Mitchell, M. Milina, J. C. Groen, J. Pérez-Ramírez, *J. Phys. Chem. C* **2011**, *115*, 14193.
[40] D. Verboekend, J. Pérez-Ramírez, *Chem. Eur. J.* **2011**, *17*, 1137.
[41] J. A. Lercher, A. Jentys, A. Brait, *Molecular Sieves*, Vol. *6*, **2008**, Springer, Berlin, pp. 201–202.
[42] M. J. Climent, A. Corma, R. Guil-Lopez, S. Iborra, *Catal. Lett.* **2001**, *74*, 161.
[43] I. Rodriguez, S. Iborra, A. Corma, F. Rey, J. L. Jordá, *Chem. Commun.* **1999**, 593.
[44] A. C. Oliveira, L. Martins, D. Cardoso, *Microporous Mesoporous Mater.* **2009**, *120*, 206.